Analysis of a Solid-State Conformational Rearrangement Using ^{15}N NMR and X-ray Crystallography

Gary McGeorge, Robin K. Harris,* Andrei S. Batsanov, and Andrei V. Churakov

Department of Chemistry, University of Durham, South Road, Durham DH1 3LE, U.K.

A. Margaret Chippendale

Zeneca Specialties Research Centre, PO Box 42, Hexagon House, Blackley, Manchester M9 8ZS, U.K.

James F. Bullock

BASF plc Textile Colours Research, PO Box 4, Earl Road, Cheadle Hulme, Cheshire SK8 6QG, U.K.

Zhehong Gan

Laboratorium für Physikalische Chemie, Eidgenössische Technische Hochschule, CH-8092 Zürich, Switzerland

Received: December 16, 1997; In Final Form: March 3, 1998

A solid azobenzene dyestuff has been studied by a combination of single-crystal X-ray diffraction and ^{15}N CP/MAS NMR. The X-ray work establishes that the crystal structure of one polymorph is disordered. The ^{15}N NMR proves that this is a temporal, rather than a spatial, effect. Three ^{15}N-enriched isotopomers (together with a second polymorph) were examined by NMR, and assignments established by rotational resonance. The shielding tensor components were determined, and the angles of change between their orientations were established by a two-dimensional exchange experiment, the theory of which is discussed. Exchange rates were measured both by selective polarization inversion and by band shape analysis. Thermodynamic parameters for the barrier to exchange are presented. It is demonstrated, by the combination of X-ray and NMR work, that the process is essentially a crankshaft motion of the azo linkage.

1. Introduction

NMR has become an immensely powerful technique for the analysis of solid-state dynamics and molecular structure. Early in the development of NMR it was realized that rapid motional processes occur in the solid state, providing relaxation sources when the rates are similar to the Larmor frequency of the nucleus under investigation.[1] Large-amplitude motions in solids, such as 180° phenyl ring flips, have been studied by NMR.[2] Dynamic processes in both organic and inorganic solids have been observed, and the vast array of publications on the subject holds testimony to this fact.

The utilization of single-crystal X-ray diffraction techniques in combination with solid-state NMR has proven to be extremely powerful. The molecular-level structure of the system can be intimately probed using the diffraction analysis, but temporal and positional disorder can remain undetected or undifferentiated. Additionally, disordered systems can prove difficult to crystallize, and this often prevents an X-ray determination of such structures. Even when sufficiently large crystals are produced, the structure cannot generally be refined simply, high accuracy on the atomic parameters being difficult to obtain. The NMR spectra, however, can be significantly influenced by the presence of motional processes and can be obtained without the requirement for single crystals. The two techniques complement each other for a full structural determination of crystalline materials.

Recently, static two- and three-dimensional exchange spectroscopy has been applied to carefully chosen systems, yielding the relative orientations of a motional axis and the principal axis systems of the affected shielding tensors. Prior to these multidimensional sequences, only simple systems with very few lines could be fully analyzed.[1,3,4] Spectra of static solids are generally broad powder patterns, so that high-resolution spectra are desired to resolve the spectral overlap for multiple-site systems. Under rapid sample rotation about the magic angle (MAS), these powder patterns decompose into a series of narrow lines centered at the isotropic shift and separated by the spinning rate. The anisotropic information is thus encoded into the intensity of individual sidebands. MAS greatly improves the sensitivity and resolution obtainable from solid-state NMR, and the 2D rotor-synchronized exchange experiment was consequently developed to study slow molecular reorientation and chemical exchange processes.[5−7] Recently it has been applied to investigate molecular conformations through polarization transfer.[8,9]

The family of donor−acceptor azobenzene dyes, classed as disperse dyes, discussed in this paper has been extensively studied in the solution state by NMR and visible spectroscopy. Very few samples have been examined in the solid state via either NMR or diffraction techniques. However, Chippendale et al.[10] have analyzed a series of disperse dyes using solid-state ^{13}C NMR and have suggested that rotation of the individual phenyl rings is hindered in the crystal environment.

We present below results obtained from the application of solid-state ^{15}N NMR spectroscopy to polymorph A of a

* To whom correspondence should be addressed. Phone: +44-(0)191−374−3121. Fax: +44-(0)191−386−1127. E-mail: r.k.harris@durham.ac.uk.

S1089-5639(98)00543-X CCC: $15.00
Published on Web 04/28/1998

SCHEME 1: Molecular Structure of I

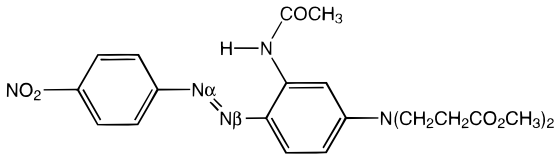

previously reported ^{15}N-enriched azobenzene dyestuff, 2′-acetamido-4′-[*N*,*N*-bis(2-methoxycarbonylethyl)amino]-4-nitroazobenzene, **I** (Scheme 1), which undergoes conformational exchange in the solid state.[11] The range of the kinetics analysis is maximized by the application of a complete band shape analysis at elevated temperatures, together with the use of the selective polarization inversion (SPI) sequence[12] at reduced temperatures. The SPI sequence is the 1D equivalent of the 2D EXSY sequence, introduced by Jeener et al.[13] The use of the 1D SPI sequence reduces the required time for the kinetics analysis considerably in comparison to 2D EXSY. The relative orientation of the ^{15}N shielding tensors of the azo Nβ and Nα sites in **I** and the change of the shielding tensor orientations caused by the molecular exchange between conformations 1 and 2 are investigated by the 2D MAS exchange experiment. In the ^{15}N doubly labeled sample, the exchange cross-peaks are either caused by the molecular exchange between the two conformations or induced by the polarization transfer between the two labeled sites through the direct dipolar coupling between two nuclear spins. With a moderate magic-angle spinning frequency, the four resonance lines of the ^{15}N doubly labeled sample become resolved, while the shielding tensor information is retained in the relative intensities of spinning sidebands. The improvement of spectral resolution and sensitivity allows the extraction of shielding tensor orientations from the 2D spinning sideband cross-peak intensities in a pairwise manner. A full solution of the crystal structure has also been determined for the same polymorph, which provides complementary information regarding the conformational rearrangement that occurs in the crystal frame of reference. The NMR evidence of exchange throws light on the disorder indicated by the X-ray results.

2. Experimental Section

Sample Preparation. Samples of **I** were prepared by N. Hall of BASF-plc, with the α and/or β azo sites enriched to ~95% with ^{15}N to create three types of isotopomer: i.e., labeled at (1) the α position, (2) the β position, and (3) both α and β positions. The polymorphic form was determined as discussed previously by X-ray powder diffraction.[11] Four samples in all have been utilized, with all three isotopomers of polymorph A being prepared, but polymorph C being labeled at the β position only. These samples are denoted by Aα, Aβ, A$\alpha\beta$, and Cβ, according to polymorphic form and position of labeling.

X-ray Diffraction. A suitable single crystal of form A was obtained by recrystallization from a 50/50 mixture of CD_2Cl_2 and MeOH over a period of a month. The resultant thin needlelike crystals proved to be relatively poor diffractors, but data collection was possible at both ambient temperature (293 K) and at 150 K. The diffraction experiments were carried out on a Rigaku AFC6S four-circle diffractometer with a Cryostream open-flow nitrogen gas cryostat, using graphite monochromated Cu Kα ($\bar{\lambda}$ =1.54184 Å) radiation. The unit cell was refined on the setting angles of 25 intense reflections with 15° < θ < 24°. The room-temperature data were corrected for absorption by the empirical method (72 azimuthal scans of 2 reflections, minimum and maximum transmission factors of 0.79 and 1.00) using the TEXSAN software.[14] The structure was solved by direct methods and refined by full-matrix least-squares against all positive F^2 to R = 0.070, using the SHELXTL software.[15] Additional information relating to the crystal data and structure refinement at 293 K is given in Table 1.

TABLE 1: Crystal Data and Structure Refinement for I, Obtained at 293 K

empirical formula	$C_{22}N_5O_7H_{25}$
formula weight	471.47
wavelength	1.54184 Å
crystal system	monoclinic
space group	$P2_1/c$
unit cell dimensions	a = 18.353(2) Å, α = 90°
	b = 12.230(2) Å, β = 98.40(1)°
	c = 10.475(2) Å, γ = 90°
volume	2326.0(7) Å^3
Z	4
density (calculated)	1.346 g/cm^3
absorption coefficient	0.898 mm^{-1}
crystal size	0.2 × 0.05 × 0.05 mm
index ranges	$-22 \le h \le 22$, $-15 \le k \le 1$, $-1 \le l \le 11$
reflections collected	4629
independent reflections	3398 [R(int) = 0.0908]

Solid-State NMR. The high-resolution ^{15}N CP/MAS NMR spectra were recorded at both 20.3 and 30.4 MHz on Chemagnetics CMX200 and Varian VXR300 spectrometers, respectively. The kinetics study was carried out on sample Aβ using the Varian spectrometer. Proton and ^{15}N field strengths equivalent to ~33 kHz were applied during the contact period, while retaining high-power proton decoupling with an effective field corresponding to 62.5 kHz (4 μs proton 90° pulse duration) during the ^{15}N signal detection and evolution periods of the exchange sequences described below. Other spectrometer operating conditions used were spectral width, 45 kHz; contact time, 10 ms; recycle delay, 2−20 s. The Hartmann−Hahn matching conditions, referencing, and angle-setting were carried out using 20% doubly enriched NH_4NO_3, with the NO_3^- signal being externally referenced to −5.1 ppm, relative to CH_3NO_2.

The selective polarization inversion sequence used involves the creation of transverse magnetization via standard cross-polarization. A nonequilibrium distribution is formed by inversion of one of the spins via a range of possible methods. For systems with a large anisotropy of the shielding tensor, as in the present azo nitrogen system, it is rather difficult to selectively invert with high efficiency over the whole sideband manifold using the DANTE or on-resonance low-power irradiation schemes, especially since the two isotropic shifts are so close. Two options exist that can eradicate this problem. One is rotor-synchronized DANTE,[16] and the other involves a specifically timed nonselective high-power pulse. The method of inversion chosen here was the second one, which was first applied to solid systems by Szeverenyi et al.,[17] whereby the ^{15}N transmitter is positioned such that the frequency offset for one resonance is twice that of the other resonance. Following the initial CP preparation, the two signals will rotate relative to the transmitter position, with one precessing twice as fast as the other. The t_1 evolution period in the 2D EXSY sequence[13] now becomes a fixed delay corresponding to $1/(2\delta\nu)$, where $\delta\nu$ is the frequency separation of the two lines. This allows the two signals to acquire a relative phase difference of π radians, which results in the signal closest to the transmitter being phase inverted. Since this technique does not involve a selective inversion pulse, it has a very high inversion efficiency, which primarily depends on the accuracy of the pulse duration. Obviously this technique would not be the one of choice if there were other lines in the spectrum involved in the exchange

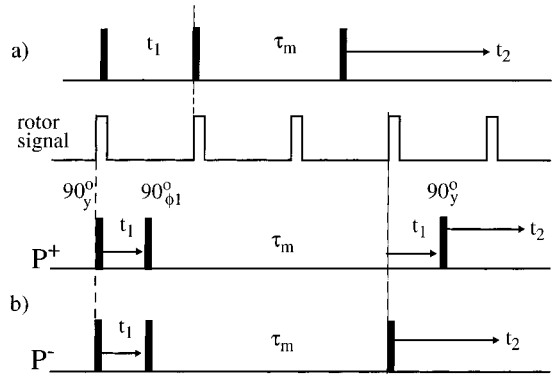

Figure 1. (a) One-dimensional analogue of the exchange sequence. Here t_1 is a fixed delay which is rotor synchronized, and τ_m is variable. (b) Rotor-synchronized pulse sequence for 2D MAS exchange spectra with pure absorptive line shapes. The beginnings of the evolution period and of the acquisition period are triggered by the rotor signal as indicated. A cross-polarization and storage sequence (not shown in the figure) is placed before the 2D pulse sequence for the enhancement of signal intensity and for shortening the recycle time. The minimum phase cycles are $\phi_1 = -y, x$, receiver $= x, -y$ for the P^+ sequence and $\phi_1 = -y, x$, receiver $= x, y$ for the P^- sequence. Additional phase cycles of the cross-polarization spin-lock pulse and of the last 90° pulse are added to the minimum phase cycles. Amplitude-modulated data sets are obtained from the two phase-modulated data sets according to Hagemeyer et al.[6] for 2D spectra with absorptive line shape.

process. The evolution time must be rotor-synchronized due to the dephasing of the magnetization from the anisotropy of the shielding tensor. The application of the second 90° pulse, which stores the magnetization along the *z* axis, should be timed so as to create this rotor-synchronization. During the mixing time, cross-relaxation occurs via exchange between the two spins, as well as from spin−lattice relaxation. After storing the magnetization for a variable mixing period τ_m, the magnetization is restored to the transverse plane and the FID is recorded. This sequence is shown in Figure 1a.

The 2D MAS exchange experiment was performed on a 300 MHz (^{1}H resonance frequency) home-built spectrometer equipped with a Chemagnetics 6 mm double-resonance MAS probe. The 2D data were acquired using the rotor-synchronized 2D exchange pulse sequence shown in Figure 1b. A cross-polarization sequence with a 7 ms contact time and subsequent magnetization storage were used (not shown in Figure 1b) to enhance the signal intensity and to shorten the recycle delay to 10 s. The ^{1}H and ^{15}N rf field strengths were both equivalent to 42 kHz during the cross-polarization, but the ^{1}H rf field strength was raised to 55 kHz for the proton decoupling. A total of 256 t_1 increments with a 20 μs dwell time was acquired for the 2D data. The total data collection time was 23 h, with 16 transients per increment. The MAS spinning rate was regulated (at 3000 ± 1 Hz) with a Chemagnetics MAS speed controller, and the TTL signal from the speed controller was used to trigger the pulse sequence shown in Figure 1b. The pure absorptive 2D spectrum was processed using the Felix software (Biosym/MSI, San Diego), following the scheme described by Hagemeyer et al.[6]

3. Calculation of Spinning Sideband Cross-Peak Intensity

In the presence of orientation-dependent shielding, the chemical shift is modulated for a sample spinning at the magic angle with frequency ω_r[18,19]

$$\omega_a(t) = \omega_a(\alpha, \beta, \psi(t)), \quad \text{where } \psi(t) = \omega_r t + \gamma \qquad (1)$$

In eq 1, (α, β, γ) are the Euler angles from the molecular-fixed frame to the initial ($t = 0$) rotor-fixed frame. The isotropic chemical shift, which merely changes the position of the spinning sideband array in the spectrum, is dropped in eq 1 because its value does not affect the spinning sideband intensity distribution. The evolution of spin magnetization under the chemical shift $\omega_a(t)$ is described by the phase factor

$$g_a(t_2, t_1) = \exp\left[i\int_{t_1}^{t_2}\omega_a(t)\,dt\right] = f_a(\omega_r t_2 + \gamma) f_a^*(\omega_r t_1 + \gamma) \qquad (2)$$

with the function

$$f_a(\psi) = \exp\left[\frac{i}{\omega_r}\int_0^{\psi}\omega_a(\alpha, \beta, \psi')\,d\psi'\right] \qquad (3)$$

The function $f_a(\psi)$ is cyclic with a period of 2π and can be expanded in a Fourier series,

$$f_a(\psi) = \sum_{k=-\infty}^{\infty} F_k^a e^{ik\psi}$$

$$F_k^a = \frac{1}{2\pi}\int_0^{2\pi} f_a(\psi) e^{-ik\psi}\,d\psi \qquad (4)$$

The contribution of a single spin to the free induction decay can be expressed as

$$g_a(t, 0) = \sum_{k,l=-\infty}^{\infty} F_k^a (F_l^a)^* e^{i(k-l)\gamma} e^{ik\omega_r t} \qquad (5)$$

It is apparent that the frequency-domain spectrum of $g_a(t, 0)$ consists of an array of spinning sidebands with intensity

$$I_k^a(\alpha, \beta, \gamma) = \sum_{l=-\infty}^{\infty} F_k^a (F_l^a)^* e^{i(k-l)\gamma} \qquad (6)$$

from a single-spin contribution. The superposition of (α, β, γ) leads to the spinning sideband intensity

$$S_k^a = \frac{1}{4\pi}\int_0^{2\pi} d\alpha \int_0^{\pi} \sin\beta\,d\beta\, F_k^a (F_k^a)^* \qquad (7)$$

for a powder sample. It is apparent from eq 7 that all spinning sidebands have pure absorptive line shape.

During the mixing period of the 2D rotor-synchronized MAS exchange pulse sequence, the molecular exchange process changes the shielding tensor from *a* to *b*, say, or the spin magnetization is transferred from spin *a* to *b*. After the accumulation of transients with the two-step phase cycles listed in Figure 1b, one obtains for the P^+ sequence the time-domain exchange signal contribution,

$$G_{ab}^+(\alpha, \beta, \gamma) = f_a(\omega_r t_1 + \gamma) f_a^*(\gamma) f_b(\omega_r t_2 + \omega_r t_1 + \gamma) f_b^*(\omega_r t_1 + \gamma) \qquad (8)$$

With the Fourier expansion in eq 4, $G_{ab}^+(\alpha, \beta, \gamma)$ can be expressed as

$$G_{ab}^+(\alpha, \beta, \gamma) = \sum_{k,l,m,n=-\infty}^{\infty} F_k^a (F_l^a)^* F_m^b (F_n^b)^* e^{i(k-l+m-n)\gamma} e^{i(k+m-n)\omega_r t_1} e^{im\omega_r t_2} \qquad (9)$$

The expansion leads to the following expression for the 2D spinning sideband cross-peak intensity from a single-spin contribution:

$$I_{ab}^{MN}(\alpha, \beta, \gamma) = \sum_{k,l=-\infty}^{\infty} F_k^a(F_l^a)^* F_N^b(F_{k+N-M}^b)^* e^{i(M-l)\gamma} \quad (10)$$

where M and N are the spinning sideband orders along the ω_1 and ω_2 dimensions, respectively.

For molecular exchange processes, the exchange amplitude for mixing time τ_m is normally independent of the molecular orientation. For polarization-transfer processes, the transfer amplitude approaches a uniform distribution when an equilibrium of spin polarization is reached among the coupled sites with a sufficiently long mixing time. The superposition of a uniform exchange signal contribution with respect to (α, β, γ) yields the spinning sideband cross-peak intensity

$$S_{ab}^{MN} = \frac{1}{4\pi}\int_0^{2\pi} d\alpha \int_0^{\pi} \sin\beta \, d\beta \sum_{k=-\infty}^{\infty} (F_M^a)^* F_N^b F_k^a (F_{k+N-M}^a)^*$$

$$= \frac{1}{4\pi}\int_0^{2\pi} d\alpha \int_0^{\pi} \sin\beta \, d\beta (F_M^a)^* F_N^b G_{M-N}^{ab} \quad (11)$$

for a powder sample. G_k^{ab} is the same Fourier expansion coefficient as in eq 4 but for the chemical shift difference of spins *a* and *b*,

$$G_k^{ab} = \frac{1}{2\pi}\int_0^{2\pi} \exp\left[\frac{i}{\omega_r}\int(\omega_a(\alpha\beta, \psi') - \omega_b(\alpha\beta, \psi'))\, d\psi'\right] e^{-ik\psi} \, d\psi \quad (12)$$

In the absence of magnetization exchange, $G_{M-N}^{aa} = \delta_{MN}$; therefore only the spinning sideband diagonal peaks have nonvanishing intensities. It should be noted that in general all the spinning sideband cross-peaks are real for powder samples,[9] and therefore a pure absorptive 2D spectrum can be obtained from an additional data acquisition using the P^- sequence in Figure 1b for the construction of amplitude-modulated time-domain data following the scheme described by Hagemeyer et al.[6]

The 2D spinning sideband cross-peak intensities are sensitive to the difference of the shielding tensors of the exchange sites. The off-diagonal spinning sideband cross-peaks, $M \neq N$, appear only when two shielding tensors are different. The difference depends not only on the principal values of the two shielding tensors but also strongly on their relative orientations. Thus, the 2D MAS exchange experiment is a particularly suitable technique to probe the shielding tensor orientations, which are normally not available from the 1D spectral line shape of powder samples.

4. Results and Discussions

Single-Crystal X-ray Analysis. In refining the structure obtained from the room-temperature data it was found that there is a single molecule in the asymmetric unit, but that N(1), N(2), and C(1) to C(6) of the phenylene ring are disordered over two positions (Figure 2), occupying virtually the same volume. Note that the designations N(1) and N(2), used in discussion of the X-ray results, correspond to Nβ and Nα, respectively. The occupancies of the two sites were refined to 47% and 53% for the conformations 1 and 2 shown in Figure 2. As a result, the azo group is seen to be disordered between two trans conformations. This is as suggested in our previous paper,[11] which investigated structural features using ^{13}C CP/MAS NMR. The structure determined at 150 K showed virtually the same geometrical arrangement, with the occupancies of conformations 1 and 2 being 53% and 47%, respectively. Only the geometrical features of the room-temperature structure will be discussed since it is thought that a poorer quality crystal was used in the 150 K experiment, resulting in a reduced signal-to-noise ratio. Conformation 1 is stabilized by formation of an intramolecular N(3)−H···N(2) hydrogen bond. For the idealized position of the hydrogen atom, the H···N(2) distance is 2.13 Å, the N(2)···N(3) distance is 2.79 Å, and the N(3)−H···N(2) angle is 133°. Consequently, a six-membered ring is formed by the hydrogen-bond formation, which presumably additionally stabilizes the system by promoting planarity of the whole molecule. Additionally, at room temperature the O(3) and O(4) sites were considered to be disordered over two positions, with occupancies refined to 35% and 65%, and at 150 K the presence of slightly elongated ellipsoids indicated the presence of the same disorder, but significantly reduced in magnitude.

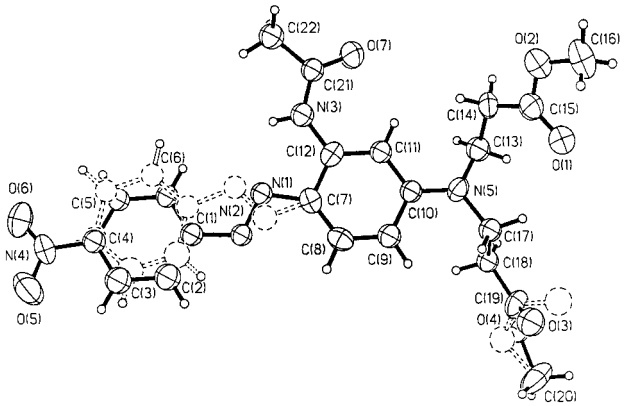

Figure 2. ORTEP plots of the two molecular conformations for the X-ray structure determination of **I** at 293 K. Thermal ellipsoids are shown at 30% for clarity, with conformer 2 being represented by the solid lines.

The X-ray results establish the fact of disorder, but are unable to distinguish between spatial and temporal effects. The occupancies are relatively close to one another at both temperatures used. However, the ^{13}C NMR results reported previously[11] and, even more definitively, the ^{15}N NMR discussed below establish unequivocally that the disorder is temporal (i.e., dynamic) in nature. On the other hand, the one-dimensional NMR experiments do not necessarily give information about the structural features between which the exchange occurs. In the present case, for instance, the NMR observations could be explained by rotation of the amino-substituted aromatic ring about the C−Nβ bond (though of course that seems unlikely because of steric hindrance from intermolecular interactions). Thus the combination of MAS NMR and X-ray crystallography proves that the motion in question is effectively a crankshaft rotation of the azo group (or, alternatively, but less likely energetically, a simultaneous in-plane inversion at both nitrogen centers). The X-ray information can then be compared with the analysis of the two-dimensional NMR data, delimiting the spatial change of the ^{15}N shielding tensors. The combination of single-crystal X-ray and ^{15}N CP/MAS spectra is thus shown to be exceedingly powerful.

The conjugation, which extends over both aromatic rings, the azo group, and the nitro group, results in an essentially planar system (ignoring the ester chains at N(5)). The deviations from the mean plane of the molecule are 2.7° and 4.3° for conforma-

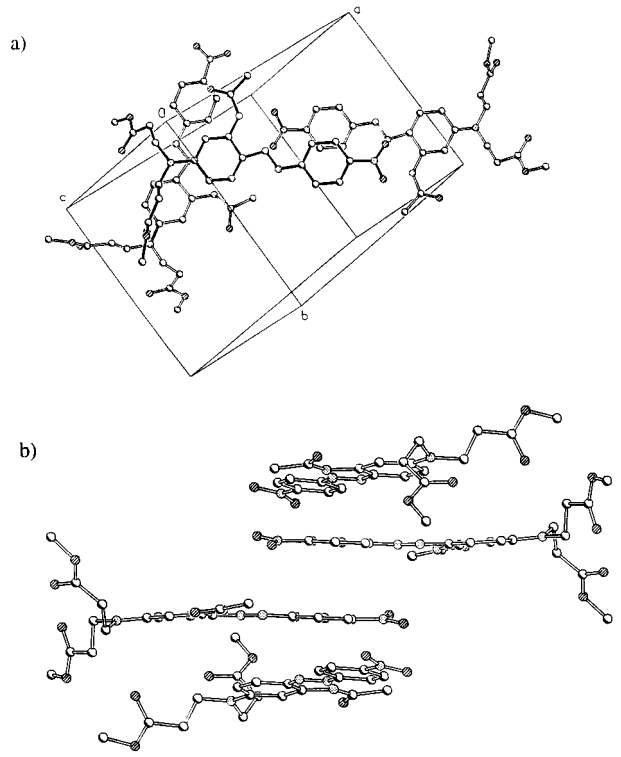

Figure 3. Molecular packing for the structure of **I**: (a) projection on the (2 0 1) plane; (b) view down this plane. Only one conformer is shown in each case for simplicity.

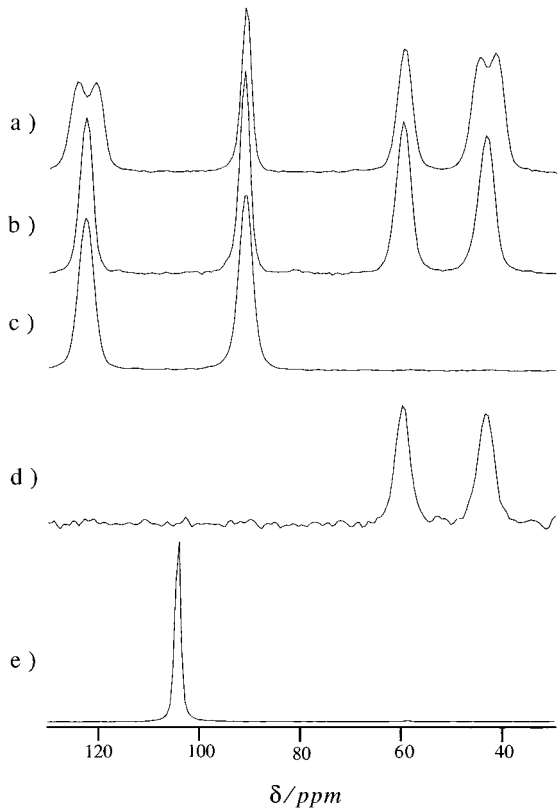

Figure 4. Nitrogen-15 CP/MAS spectra for the labeled samples of polymorph A of **I**: (a) α,*β* double label at a spin rate of 2330 Hz, which corresponds to the $n = 1$ rotational resonance condition; (b) α,*β* double label in the high-speed limit; (c) *β* single label; (d) α single label, and also for polymorph C of **I**; (e) *β* single label.

tion 1 and 14.7° and 3.7° for conformation 2, about the C(1)−N(2) and N(1)−C(7) bonds, respectively. The ester chain also prevents the formation of a regular stacking arrangement of the entire molecule, but it is possible to discern partial stacks (Figure 3). They include pairs of antiparallel C(1−6) and C(7−12) aromatic rings with an interplanar separation of approximately 3.3 Å, which is typical for $\pi-\pi$ stacking. These dimers are interleaved by amido groups.

It should be noted that many phenylazobenzenes crystallize in the monoclinic crystal system, with similar cell dimensions. Such structural mimicry is commonplace for structures based mainly on van der Waals interactions. Thus, molecules that exhibit similar van der Waals surfaces crystallize in similar arrangements, provided that hydrogen-bonding interactions do not dominate in the crystal formation. For example, the analogous *trans*-stilbene[20] and *N*-salicylideneaniline[21] molecules are both known to crystallize with the $P2_1/c$ space group. Single-crystal X-ray diffraction studies have been carried out at room temperature on the parent molecule *trans*-azobenzene[22] and the next homologue *p*-azotoluene,[23] with both molecules showing similar disordered arrangements. Two conformations for each molecular system were found, with essentially different orientations of the azo linkage, just as in the present structure determination. Those diffraction experiments did not yield information relating to the nature of the disorder, since it is not possible to distinguish between spatial and temporal cases at one temperature. An investigation by Harada et al.,[24] published while the present paper was in the final stages of preparation, utilized X-ray crystallography at temperatures below 100 K to elucidate the disordered nature of *trans*-azobenzene and three methylated derivatives. Their results showed a change of the fractional populations of two disordered sites as a function of temperature, ultimately freezing out the disorder in *trans*-azobenzene at 80 K, thus verifying that for the species investigated the disorder was dynamic in nature. For *p*-azotoluene we have observed broadened peaks for C(2) and C(6) in the ^{13}C CP/MAS spectra at room-temperature, resulting from a slow conformational rearrangement (see also ref 10). Upon raising the temperature the two peaks collapse into a closely separated doublet, under the typical two-site exchange phenomenon. The fact that the lines collapse into a doublet is presumably a result of the fact that the packing around the phenyl group is not symmetric in the crystal. The disorder observed in the crystal structure may be associated with a similar motional process as investigated here for **I**.

Harada et al.[24] suggested that the conformational exchange was mediated via a vibrational motion of the N-phenyl bonds, and if the vibration amplitude was sufficiently large, then it was possible for a conformational jump to occur. Furthermore, the vibrational motion produced a transient (transition) conformation where the azobenzene moiety was arranged perpendicular to the phenyl ring planes.

Nitrogen-15 NMR. The ^{15}N solid-state CP/MAS NMR spectra of Aα, A*β*, Aα*β*, and C*β* are shown together in Figure 4. The spectra of the two singly labeled samples of polymorph A both display the presence of the two conformations, with shifts of 60 and 44 ppm for Aα and 121 and 89 ppm for A*β*. These are sufficiently separated in each case that it is clear the origin is not the existence of two molecules with similar conformations in the asymmetric unit. The spectrum of isotopomer Aα*β* appears to be simply a superposition of those for the two singly labeled samples. The ^{15}N shift of 105.4 ppm for sample C*β* appears not to correlate to the same structure as those for polymorph A, which is actually as expected from consideration of the ^{13}C spectra.[11] Polymorph C was thought to be present in the non-hydrogen-bonded conformation, with the acetamide group rotated out of the plane associated with the azobenzene

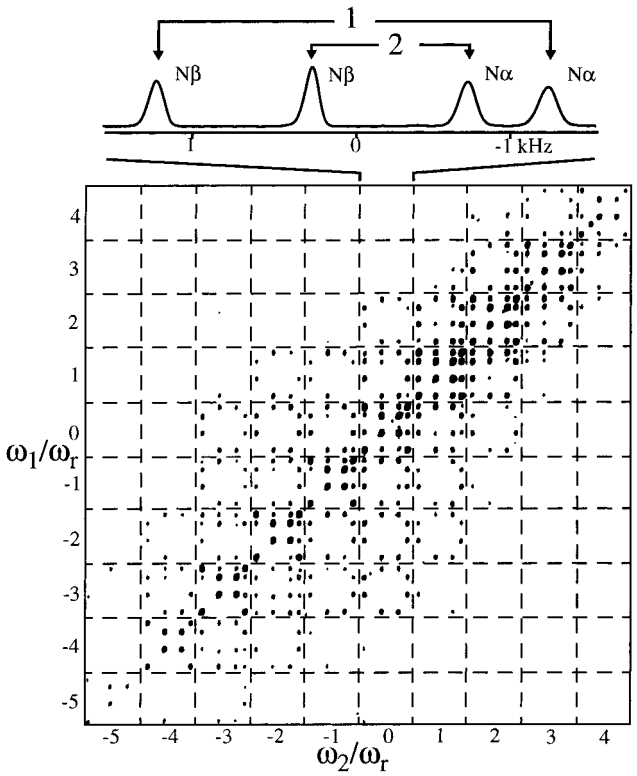

Figure 5. Contour plot of the 2D MAS exchange spectrum for the ^{15}N doubly labeled sample A$\alpha\beta$ at 283 K with a 2 s mixing time. The expanded 1D spectrum in the central spinning sideband region is also plotted along with the peak assignments.

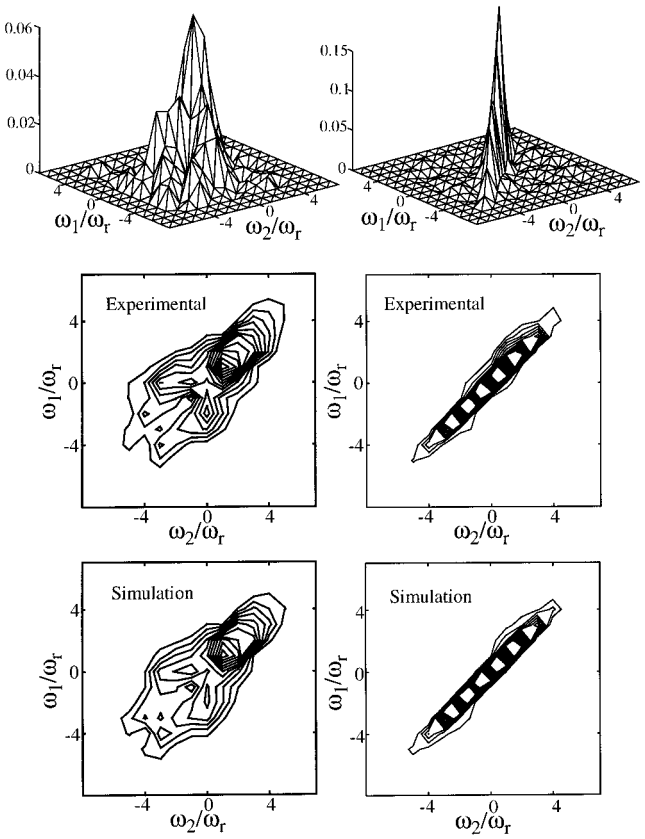

Figure 6. Experimental and simulated 2D spinning sideband intensity distributions for sample A$\alpha\beta$. The left side corresponds to exchange of the Nβ site between the molecular conformations 1 and 2, and the right side is for the Nβ and Nα sites in conformation 1. The top and middle figures show the surface plot and the contour plot of the experimental measurements. The bottom figures are the best-fit simulations with values of $\theta = 37°$ and $\theta = 5°$ for the left and right plots, respectively.

moiety. Such a reorientation would alter the electronic overlap between the azo nitrogen system and the acetamide group. The local geometry infers that, in the non-hydrogen-bonded conformation, the α azo site is spatially far removed from the acetamide group, and thus its chemical shift would be influenced only slightly by the acetamide system. However, the β site is only approximately 3.5 Å away from the acetamide group, and consequently any reorientations would alter the electronic environment of the β nuclear site. The natural-abundance α resonance for polymorph C is coincident with that of the 60 ppm resonance for one of the α sites for polymorph A. Thus, the resonances at 60 and 44 ppm can be assigned to the non-hydrogen-bonded and hydrogen-bonded conformations, respectively.

This, however, does not help in the assignment of the Aβ sample on which the kinetics analysis was carried out (see below). This problem was addressed by consideration of the fact that sample A$\alpha\beta$ contains an isolated ^{15}N−^{15}N homonuclear spin-pair. Under magic-angle spinning, dipolar couplings are averaged to their isotropic value, which is zero. These couplings can be reintroduced by the application of the rotary resonance technique (R^2) used to measure homonuclear dipolar coupling constants.[25−27] This technique involves matching the spin rate to the chemical shift separation, in hertz, between the two coupled spins, resulting in a scaled dipolar/chemical shift powder pattern.

In the present case, matching the spin rate to the separation between the 121 and 60 ppm resonances should reintroduce the dipolar coupling if these two resonances are from spins present within the same molecule. This separation, at a ^{15}N Larmor frequency of 30.5 MHz, is ∼1860 Hz. However, the ^{15}N CP/MAS spectrum obtained at this spin rate showed very little change in line width for the relevant resonances. On the other hand, repeating the CP/MAS spectrum at a spin rate of 2330 Hz, corresponding to matching the 121 and 44 ppm resonances, resulted in a splitting of ∼200 Hz (similarly for the 89 and 60 ppm resonances). The $n = 1$ ^{15}N CP/MAS rotational resonance spectrum carried out at a spin rate of 2330 Hz is shown in Figure 4a. This result leads to the conclusion that the 121 and 44 ppm resonances arise from nuclei in the same molecule, and they can thus be assigned to the hydrogen-bonded conformation. With this assignment obtained, it became sensible to pursue the kinetics analysis.

2D Rotor-Synchronized Exchange Experiments. Figure 5 shows the 2D MAS exchange spectrum of ^{15}N doubly labeled A$\alpha\beta$ at 283 K, along with a 1D expansion of the central sideband region. The four resonances correspond to the Nβ and Nα sites in the two molecular conformations. The 2 s mixing time is sufficiently long for complete exchange between the two molecular conformations to occur and for complete polarization transfer between the two labeled sites. Spectral intensities are integrated for the cross-peaks connecting the spinning sidebands for each pair of resonance lines. Figure 6 shows the surface plot and the contour plot of a typical 2D spinning sideband intensity distribution. A maximum of 16 spinning sideband intensity distributions can be extracted from the spectrum of the four-site system. As outlined earlier, the principal components of the shielding tensor are required for the analysis of the 2D exchange spectrum. Wasylishen et al.[28] have analyzed the orientation of the shielding tensor for *trans*-azobenzene in the PAS and suggested that the σ_{22} component

TABLE 2: Principal Components of the ^{15}N Shielding Tensors for Conformations 1 and 2 of the Azo Nitrogens α and β in Polymorph A

δ_{iso}/ppm[a]	σ_{iso}/ppm	σ_{11}/ppm	σ_{22}/ppm	σ_{33}/ppm
44	−179.8	−606	−102	168
60	−195.8	−636	−113	164
89.6	−225.4	−713	−158	187
121	−256.8	−750	−168	143
131[b]	−266.8	−789	−146	136

[a] Reported relative to the signal for CH_3NO_2. The determined shifts (δ_{ii}) and shieldings (σ_{ii}) are related according to $\sigma_{ii} = -135.8 - \delta_{ii}$, where δ_{ii} are measured on the nitromethane scale and shielding components are given relative to the bare nucleus. [b] The principal components for azobenzene, as determined by Wasylishen[28] are given for comparison. The principal shielding components σ_{ii} are ordered according to $\sigma_{11} < \sigma_{22} < \sigma_{33}$ as defined by Mason.[32]

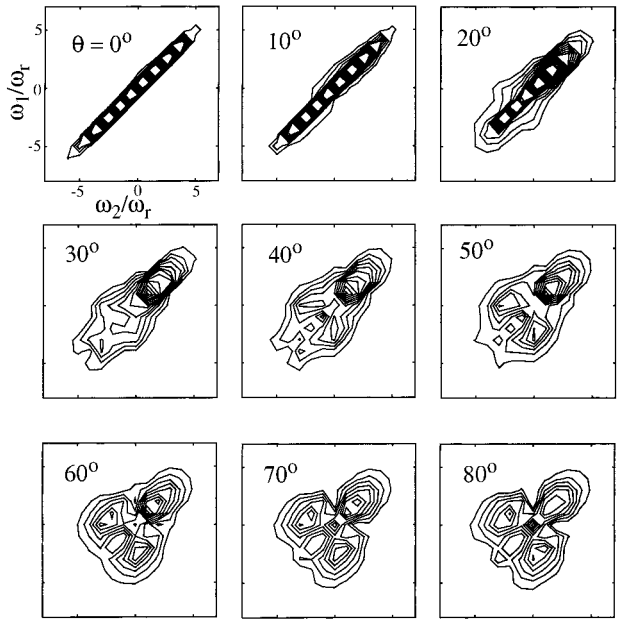

Figure 7. Contour plots of simulated spinning sideband intensity distribution for the Nβ site exchanging between molecular conformations 1 and 2 with different θ angles between the σ_{22} principal axes of the shielding tensors. σ_{33} principal axes are perpendicular to the local molecular plane.

is collinear with the lone-pair orbital and the σ_{33} component is approximately perpendicular to the plane of the azo linkage. The principal components of the ^{15}N shielding tensor for all four sites of **I**Aα*β* are given in Table 2. These values were obtained from an analysis of the static line shapes of the Aα and A*β* singly labeled samples. However, coupling to the neighboring ^{14}N nucleus was ignored because the actual values obtained for the shielding components were found to be insensitive to this coupling, which is in part due to the particular orientation of the shielding tensor relative to the dipolar vector. In comparing the principal components, it is clear that most of the difference in the shifts observed for the isotropic values is associated with a change in σ_{11}. This component is highly sensitive to the energy of the $n \rightarrow \pi^*$ transition, and therefore the interaction between the π system and the nonbonding electrons defines the resonance frequency.

Figure 7 shows the simulated spinning sideband intensity distribution connecting the resonance lines of the Nβ site in conformation 1 along ω_1 and in conformation 2 along ω_2. For **I**, the σ_{33} axis can be assumed to be perpendicular to the local molecular plane, and the relative tensor orientation is described by the angle θ between the two σ_{22} axes. Simulations presented in Figure 7 show the 2D spinning sideband intensity distributions for various angles θ. The strong dependence of the 2D spectra on the angle θ ensures an accurate determination of the relative shielding tensor orientations.

The best-fit simulation for the Nβ site is shown in Figure 6 and was found for $\theta = 37°$. The exchange between the two molecular conformations rotates the principal axes of the shielding tensors in the plane by 37°, and the corresponding angle for the Nα site was found to be 31°. Due to the symmetry constraints imposed upon the experiment, these angles could also be $(180 - \theta)°$, which appears realistic when one compares the results to the ORTEP plot in Figure 2. By placing the σ_{22} axes collinear with the lone-pair orbitals of the corresponding azo nitrogen, one obtains angles of 135° and 136° for the N(1) and N(2) sites, respectively, from the X-ray study, which compares to 143° and 149° from the 2D exchange results. The lone-pair orbitals were assumed to be along the vectors that bisect the N(1)−N(2)−C(7) and C(1)−N(1)−N(2) angles. Figure 6 also shows the experimental measurement and best-fit simulation of the spinning sideband intensity distribution connecting the resonance lines of Nβ and Nα sites in conformation 1. It is apparent from the figure that most of the intensities are concentrated within the cross-peaks lying along the main diagonal, indicating that the two sites have similar shielding tensors, including the principal values and the orientations of the principal axes. It should be expected that the two tensors have similar principal axes because the local environments for the two sites have nearly inversion symmetry. By comparing the simulations, the angles between the principal axes of the shielding tensors in the local plane are found to be smaller than 5° for the two conformations 1 and 2.

Kinetics Analysis. Two-dimensional experiments of the kind just discussed are in general rather time-consuming, even for the case of highly labeled samples, and so an analogous one-dimensional experiment was carried out over a large temperature range. With systems possessing a large anisotropy of the shielding tensor, one must consider the effect of the sample spinning, which further complicates the situation. Under MAS the dephasing associated with the t_1 period is primarily due to the time dependence of the resonance frequency resulting from the anisotropy of the shielding tensor. As proved by Maricq and Waugh,[18] such dephasing is only refocused at integral multiples of the rotor period, and a rotor echo occurs, forcing one to store the magnetization only at the top of a rotor echo. The temporal width of the rotor echo is inversely proportional to the static line width, and for systems with large anisotropies this fact imposes a strict rotor synchronization on the evolution period. Experimentally it was observed that the evolution time had to be a multiple of $2n$ rotor periods, where n is an integer, and that the error in the spin rate should be less than the line width of the individual sidebands (∼50 Hz). A spin rate of 3850 Hz was subsequently chosen such that $n = 2$, and a t_1 evolution time of 515 μs was used. An example of a SPI spectrum with no mixing time is given in Figure 8. During the period where the spins are relaxing according to T_1 and exchange, the signal intensity can be determined via the exchange-modified Bloch equations.

For a two-site A ⇔ B scheme the coupled differential equations for the z-magnetizations are

$$\frac{d}{dt}(M_Z^A) = -R_{A1}(M_Z^A - M_O^A) - k_f M_Z^A + k_b M_Z^B \quad (13)$$

$$\frac{d}{dt}(M_Z^B) = -R_{B1}(M_Z^B - M_O^B) - k_b M_Z^B + k_f M_Z^A \quad (14)$$

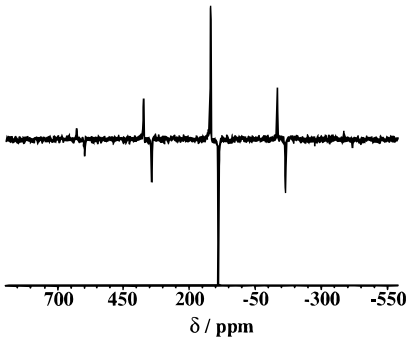

Figure 8. An example of an initial-state phase-inverted ^{15}N spectrum with no mixing time for **I**.

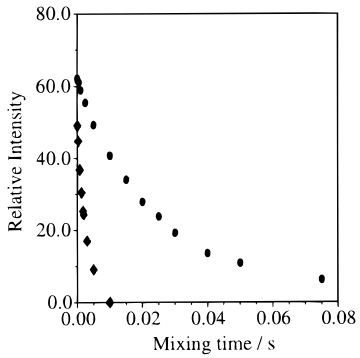

Figure 9. Experimental results for the ^{15}N SPI experiment, shown as difference curves, for sample Aβ of **I** at (diamonds) 323 K and (circles) 295 K.

where M_Z^A and M_Z^B are the z-magnetizations of sites A and B, respectively, after a mixing time of τ_m (see Figure 1), while M_O^A and M_O^B are the initial z-magnetizations. Additionally, by assuming perfect inversion of the spin system, *i.e.* $M_O^A = M_\infty^A$ and $M_O^B = -M_\infty^B$, then M_O^B becomes a negative quantity. R_{A1} and R_{B1} are the spin−lattice relaxation rates ($1/T_1$) for each site, and k_f and k_b are the forward and backward rate constants, with A ⟹ B defined as the forward process.

The ^{15}N spin−lattice relaxation time for the azo nitrogens was found to be ∼1000 ±100 s via the nonselective inversion−recovery sequence of Torchia.[29] This sequence allows for a relatively rapid repetition rate, determined by the proton T_1 relaxation time, which is generally shorter than that for the ^{15}N nucleus. The ^{15}N T_1 relaxation time is long enough to allow the exchange-modified Bloch equations to be simplified by ignoring such relaxation during the relatively short mixing times. The time evolution of the individual magnetization vectors, during the mixing time, can now be considered to be governed by first-order reaction kinetics and therefore can be fitted, for the general case of a nonintegral equilibrium constant, to a simple shifted exponential function. In the following analysis the difference of the two magnetizations was fitted as a function of mixing time:

$$M_{diff} = M_Z^A - M_Z^B = (M_O^A - M_O^B)\exp(-(k_f + k_b)t) + (M_O^A + M_O^B) \quad (15)$$

The relative sign (phase) of the magnetization vectors is retained in these equations, and as a result, the first factor is the total initial magnitude of magnetization, the second expresses the exponential recovery back to equilibrium, and the last term is the final equilibrium magnetization in the absence of T_1 relaxation. Figure 9 shows the magnetization transfer curves for the difference equation, taken at 50 and 22 °C. As can be seen, the exchange process is much faster for the higher temperature, as expected. The results from the whole temperature range are given in Table 3. The equilibrium constant K was determined from the modulus of the ratio of the two M_O^A and M_O^B coefficients. The values were obtained by linear regression of eq 15, using the software package MATHCAD.[30]

TABLE 3: Sum of the Exchange Rates, $k_f + k_b$, as a Function of Temperature from (a) the SPI Data by Fitting the Difference Magnetization (243−323 K), and (b) the Bandshape Fitting at Elevated Temperatures (328−352 K). The Forward and Backward Rates k_f and k_b Were Determined from the Sum, Together with the Equilibrium Constant *K*

T/K	k_{sum}/Hz	*K*	k_f/Hz	k_b/Hz
243	0.110	1.31	0.062	0.048
253	0.343	1.24	0.19	0.15
263	1.40	1.21	0.77	0.63
273	4.06	1.16	2.18	1.88
281	10.3	1.12	5.4	4.9
295	45.4	1.07	23.4	22.0
303	87.6	1.04	44.6	43.0
313	178	1.01	89	89
323	349	0.98	172	177
328	460	0.94	223	237
336	962	0.91	458	504
345	2260	0.88	1055	1205
352	3360	0.84	1536	1824

Further increases of the temperature resulted in a broadening of the signals, which was maximum at ∼70 °C at 30.5 MHz. This typical two-site exchange has been observed many times previously, and the resultant band shapes can be fitted according to the exchange-modified Bloch equations, which were solved by Rogers and Woodbury[31] for the simple isolated two-spin system. At the high spinning rates used (∼6 kHz) there was no overlap between the exchange−broadened sideband manifolds, and therefore the above approach can be applied without complication. The estimated values of the exchange rates are given in Table 3 along with the results from the SPI analysis.

The thermodynamic activation parameters for the molecular reorientation of **I** were determined from Eyring plots ($\ln(k_f/T)$ vs $1/T$) of the kinetics data given in Table 3 (Figure 10). Least-squares fits produced the parameters, which are summarized in Table 4 for both the forward and backward processes (use being made of the equilibrium constants listed in Table 3). These activation parameters yield information relating to the structure of the potential energy surface, which is assumed to be a double well, and therefore to the relative stabilities of the two structures. Here we assume that the transmission coefficient κ is equal to unity. The interconversion rate between the two conformations is dominated by the enthalpic contribution to the Gibbs free energy, which is as expected since the activated state is unlikely to have a significantly different entropy from the ground state. The barrier is of the same order of magnitude as for simple phenyl ring rotation, for which it has been shown in a typical case[2] that the free energy of activation is ca. 58 kJ mol^{-1}. The volume required for rotation of a phenyl group is not dissimilar to that for the diazo group. However, barriers to rotation in the solid state have important contributions from crystal packing interactions, so that comparisons between disparate cases are not particularly fruitful. This azobenzene dye has a relatively low density (1.346 g/cm^{-3}) in comparison to many other organic molecules, which implies a large free volume, thus facilitating molecular reorientation.

Molecule **I** is interesting from the fact that it possesses three polymorphs, each of which produces a distinctly different ^{13}C and ^{15}N CP/MAS spectrum.[11] These are essentially from

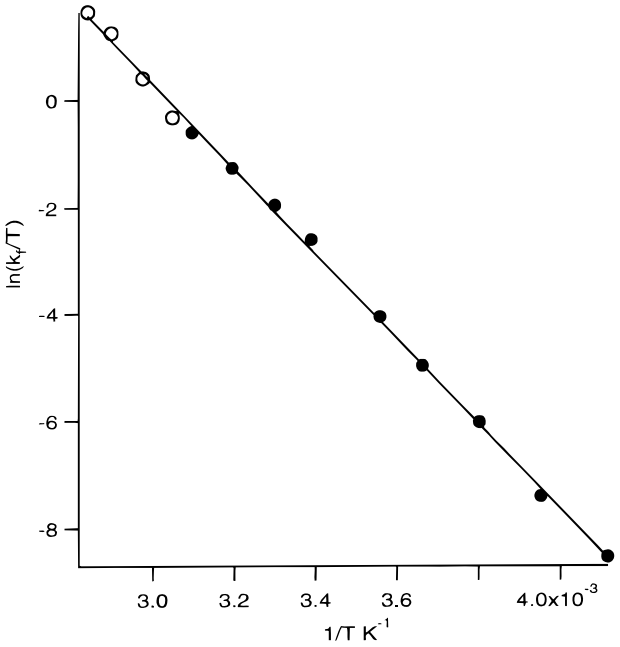

Figure 10. Eyring plot of the kinetics analysis carried out for sample Aβ of **I** using both (a) the SPI (denoted by solid circles) and (b) the band shape analysis techniques (denoted by open circles), where k_f is the exchange rate for the forward process, i.e., 121 → 89 ppm.

TABLE 4: Thermodynamic Activation Parameters Obtained for the Process Which Interconverts Conformations 1 and 2, As Derived from the Eyring Plot Shown in Figure 9

forward (121 ppm → 89 ppm)			backward (89 ppm → 121 ppm)		
$\Delta H^{\ddagger}$/ kJ mol^{-1}	$\Delta S^{\ddagger}$/ J mol^{-1} K^{-1}	$\Delta G^{\ddagger}_{298}$/ kJ mol^{-1}	$\Delta H^{\ddagger}$/ kJ mol^{-1}	$\Delta S^{\ddagger}$/ J mol^{-1} K^{-1}	$\Delta G^{\ddagger}_{298}$/ kJ mol^{-1}
63.3 (±1)	−5.8 (±2)	65.0 (±1)	65.6 (±1)	3.2 (±2)	66.6 (±1)

molecules that exhibit different conformations in the asymmetric unit, and the conformations with higher energy are presumably stabilized by crystal-packing interactions. However, polymorphs B and C have not produced single crystals suitable for X-ray analysis. Additionally, polymorph B (not discussed in the current text) shows the same resonance frequencies (same conformations) in its ^{13}C CP/MAS spectrum as that of polymorph A, but in a different proportion. Thus the equilibrium position of the disordered species can apparently be shifted by the interaction energy arising purely from crystal-packing effects, suggesting that the two crystal systems are very similar in their arrangements.

5. Conclusions

The combination of ^{15}N solid-state NMR and single-crystal X-ray diffraction has allowed a complete understanding of the disordered nature of a typical azobenzene dyestuff. The single-crystal X-ray study resolved the presence of two conformations with an approximately equal weighting within the asymmetric unit. The nature of the disorder was proved to arise from a motional process that interconverted two trans conformations on a time scale observable by high-resolution solid-state NMR. The axis of this reorientation was accurately located by application of the two-dimensional rotor-synchronized exchange sequence, with the prior knowledge of the orientations of the principal-axis systems of shielding tensors in the molecular axis frames of the azo nitrogen nuclei. Selective polarization-inversion and band shape-fitting experiments have yielded the thermodynamic parameters of the exchange process.

Acknowledgment. G.M. thanks EPSRC and Zeneca Specialties for a research studentship via a CASE award. We are also grateful to EPSRC for a research grant (GR/HR96096) which enabled purchase of the Chemagnetics CMX200 spectrometer used. We are indebted to Nigel Hall for synthesis of the labeled dyestuffs.

Supporting Information Available: The single-crystal X-ray data (12 pages) for the structures of **I**, determined at 298 and 150 K, are available. Ordering information is given on any current masthead page.

References and Notes

(1) Mehring, M. *Principles of High-Resolution NMR in Solids*, 2nd ed.; Springer-Verlag: New York, 1983.
(2) Riddell, F. G.; Bremner M.; Strange, J. H. *Magn. Reson. Chem.* **1994**, *98*, 843.
(3) Solum, M. S.; Zilm, K. W.; Milch, J.; Grant, D. M. *J. Am. Chem. Soc.* **1983**, *87*, 2940.
(4) Hoelger, C. G.; Aguilar-Parilla, F.; Elguero, J.; Weintraub, O.; Vega, S.; Limbach, H. H.; *J. Magn. Reson.* **1996**, *120*, 46.
(5) Kentgens, A. P. M.; deBorer, E.; Veeman, W. S. *J. Chem. Phys.* **1987**, *87*, 6859.
(6) Hagemeyer, A.; Schmidt-Rohr, K.; Spiess, H. W., *Adv. Magn. Reson.* **1989**, *13*, 85.
(7) Luz, Z.; Spiess, H. W.; Titman, J. J. *Isr. J. Chem.* **1992**, *32*, 145.
(8) Weliky, D. P.; Tycko, R. *J. Am. Chem. Soc.* **1996**, *118*, 8487.
(9) Tycko, R.; Weliky, D. P.; Berger, A. E. *J. Chem. Phys.* **1996**, *105*, 7915.
(10) Chippendale, A. M.; Mathias, A.; Harris, R. K.; Packer, K. J.; Say, B. J. *J. Chem. Soc., Perkin Trans. 2* **1981**, 1031.
(11) McGeorge, G.; Harris, R. K.; Chippendale, A. M.; Bullock, J. F. *J. Chem. Soc., Perkin Trans. 2* **1996**, 1733.
(12) Connor, C.; Naito, A.; Takegoshi, K.; McDowell, C. A. *Chem. Phys. Lett.* **1985**, *113*, 123.
(13) Jeener, J.; Meier, B. H.; Bachmann, P.; Ernst, R. R. *J. Chem. Phys.* **1979**, *71*, 4546.
(14) *TEXSAN*: TEXRAY Structure Analysis Package, Ver. 5; Molecular Structure Corporation: The Woodlands, TX, 1989.
(15) Sheldrick, G. M. *SHELXTL*, Ver. 5; Siemens Analytical X- Ray Instruments Inc.: Madison, WI, 1994.
(16) Caravatti, P.; Bodenhausen, G.; Ernst, R. R. *J. Magn. Reson.* **1983**, *55*, 88.
(17) Szeverenyi, N. M.; Bax A.; Maciel, G. E. *J. Am. Chem. Soc.* **1983**, *105*, 2579.
(18) Maricq M. M.; Waugh, J. S. *J. Chem. Phys.* **1979**, *70*, 3300.
(19) Herzfeld, J.; Berger, A. E. *J. Chem. Phys.* **1980**, *73*, 6021.
(20) Bouwstra, J. A.; Schouten, A.; Kroon, J.; Helmholdt, R. B, *Acta Crystallogr.* **1970**, *C41*, 420.
(21) Woznaik, K.; He, H.; Klinowski, J.; Jones, W.; Dziembowska, T.; Grech, E. *J. Chem. Soc., Faraday Trans.* **1995**, *91*, 77.
(22) Bouwstra, J.; Schouten, A.; Kroon, J. *Acta Crystallogr.* **1983**, *C39*, 1121.
(23) Brown, C. J. *Acta Crystallogr.* **1966**, *21*, 146.
(24) Harada, J.; Ogawa, K.; Tomoda, S. *Acta Crystallogr.* **1997**, *B53*, 662.
(25) Levitt, M. H.; Raleigh,D. P.; Creuzet, F.; Griffin, R. G. *J. Chem. Phys.* **1990**, *92*, 6347.
(26) Challoner, R.; Harris, R. K. *Chem. Phys. Lett.* **1994**, *228*, 589.
(27) Bennett, A. E.; Griffin R. G.; Vega, S. J. *NMR Basic Principles Prog.* **1994**, *33*, 1.
(28) Wasylishen, R. E.; Power, W. P.; Penner, G. H.; Curtis, R. C. *Can. J. Chem.* **1989**, *67*, 1219.
(29) Torchia, D. A. *J. Magn. Reson.* **1986**, *30*, 613.
(30) *MATHCAD Plus 6*; Mathsoft Inc., 1995.
(31) Rogers, M. T.; Woodbury, J. C. *J. Phys. Chem.* **1962**, *66*, 540.
(32) Mason, J. *Solid State NMR* **1993**, *2*, 285.